Annealing-Tunable Charge Density Wave in the Magnetic Kagome Material FeGe

Xueliang Wu,[1,*] Xinrun Mi,[1,*] Long Zhang,[1,*] Chin-Wei Wang,[2] Nour Maraytta,[3] Xiaoyuan Zhou,[1] Mingquan He,[1,†] Michael Merz,[3,4,‡] Yisheng Chai,[1,§] and Aifeng Wang[1,‖]

[1]*Low Temperature Physics Laboratory, College of Physics and Center of Quantum Materials and Devices, Chongqing University, Chongqing 401331, China*

[2]*National Synchrotron Radiation Research Center, Hsinchu 300092, Taiwan*

[3]*Institute for Quantum Materials and Technologies, Karlsruhe Institute of Technology, Kaiserstraße 12, 76131 Karlsruhe, Germany*

[4]*Karlsruhe Nano Micro Facility, Karlsruhe Institute of Technology, Kaiserstraße 12, 76131 Karlsruhe, Germany*

The unprecedented phenomenon that a charge density wave (CDW) emerges inside the antiferromagnetic (AFM) phase indicates an unusual CDW mechanism associated with magnetism in FeGe. Here, we demonstrate that both the CDW and magnetism of FeGe can be effectively tuned through postgrowth annealing treatments. Instead of the short-range CDW reported earlier, a long-range CDW order is realized below 110 K in single crystals annealed at 320 °C for over 48 h. The CDW and AFM transition temperatures appear to be inversely correlated with each other. The onset of the CDW phase significantly reduces the critical field of the spin-flop transition, whereas the CDW transition remains stable against minor variations in magnetic orders such as annealing-induced magnetic clusters and spin-canting transitions. Single-crystal x-ray diffraction measurements reveal substantial disorder on the Ge1 site, which is characterized by displacement of the Ge1 atom from the Fe_3Ge layer along the c axis and can be reversibly modified by the annealing process. The observed annealing-tunable CDW and magnetic orders can be well understood in terms of disorder on the Ge1 site. Our study provides a vital starting point for the exploration of the unconventional CDW mechanism in FeGe and of kagome materials in general.

The interplay of lattice geometry, nontrivial band topology, and electronic correlations in a kagome lattice could lead to diverse emergent quantum phases of matter [1–3]. A notable example is the kagome metals AV_3Sb_5 (A = K, Rb, Cs), which has attracted great attention due to the observation of abundant intertwined electronic orders such as nontrivial band topology, CDW, superconductivity, nematicity, and pair density wave [4–9]. The recent discovery of CDW order in the magnetic kagome metal FeGe (hexagonal, B35) adds further interest to this field [10]: In stark contrast to AV_3Sb_5 and other CDW materials, the CDW state of FeGe appears deep inside the antiferromagnetic phase, suggesting an unconventional CDW mechanism intertwined with magnetism [10].

Despite showing the same 2×2 charge modulation [10–12], FeGe and AV_3Sb_5 differ significantly in structural distortions. In AV_3Sb_5, CDW emergence is tied to in-plane distortions within the V-kagome plane and accompanied by phonon instabilities [13], likely driven by Fermi surface nesting (FSN) of Van Hove singularities (VHSs) [14–18]. Conversely, the CDW in FeGe features dimerization of Ge1 atom along the c axis without showing imaginary phonon modes in the pristine phase [19–21]. Nonetheless, FSN of kagome states might also drive the CDW transition in FeGe [21,22]. However, the VHS is limited to a narrow k_z window near E_F, and electron-electron correlations might play important roles [23,24]. Furthermore, recent photoemission experiments have not shown clear evidence of FSN and gap opening near E_F [25]. Alternatively, a balance between structural distortion versus magnetic exchange energy, or Peierls-like effects associated with Ge1 bands, can lead to a double- or triple-well energy landscape [26,27]. Such a landscape might account for both the structural distortion and the driving force of the CDW transition. Despite these various proposed mechanisms, the exact nature of the CDW remains elusive so far.

The exploration of the intrinsic CDW mechanism in FeGe is greatly complicated by discrepancies found experimentally: In early reports, no other transitions were found, except magnetic ones, in the hexagonal phase of FeGe [28–31]. In recent neutron and scanning tunneling microscopy (STM) studies, a short-range CDW state with a second-order-like transition was discovered [10–12]. On the other hand, x-ray scattering experiments indicate that the CDW is long-ranged and its transition is weakly first order [20]. The weak CDW signatures and strong sample dependence hamper the investigation of the underlying mechanisms. To settle the experimental discrepancies, and to probe the intrinsic properties, it is of prime importance to prepare high-quality FeGe crystals that show clear and tunable CDW signatures.

During the single-crystal growth processes of FeGe, we found that enhancing the CDW signal by varying growth

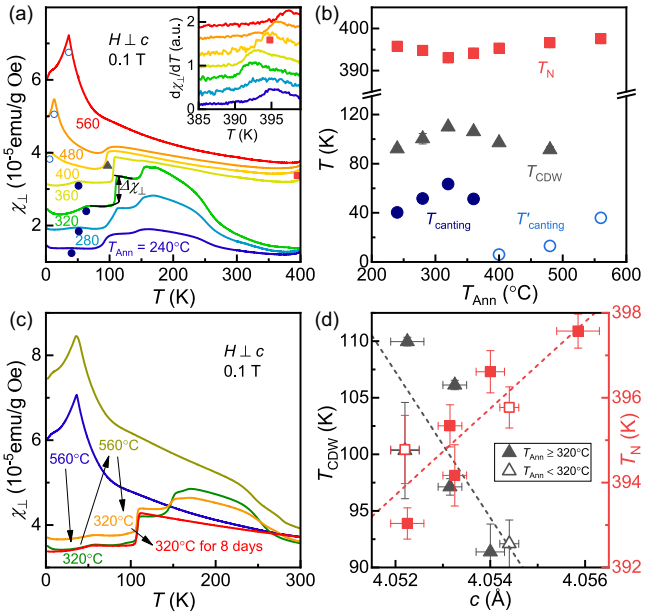

FIG. 1. (a) Temperature-dependent in-plane magnetic susceptibilities of FeGe samples annealed at different temperatures for 48 h, measured under a 0.1 T magnetic field using zero-field cooling (ZFC) mode. The curves in (a) have been shifted vertically for clarity. The AFM, CDW, and canting transitions are marked by red squares, gray triangles, and blue circles. The inset in (a) shows the temperature derivative of $\chi_\perp(T)$ near T_N. (b) Phase diagram of various transition temperatures tuned by the annealing temperature. (c) $\chi_\perp(T)$ of a FeGe crystal annealed in the sequence of 560-320-560-320 °C (48 h each) alongside a sample annealed at 320 °C for 8 day (red curve). (d) Correlation of T_{CDW} and T_N with the c-axis lattice parameters. Lattice parameters were obtained from powder x-ray diffraction measurements with a LaB_6 standard (Fig. S2 in Supplemental Material [32]). Dashed lines are guides to the eye. Note: Error bars in panels (b) and (d) are identical, but are not visible in (b) due to large symbol sizes.

conditions turned out to be challenging. In this Letter, we demonstrate the ability to systematically and repeatably adjust the CDW from short-ranged to long-ranged by employing postgrowth annealing in vacuum at temperatures ranging from 240 to 560 °C, with subsequent rapid quenching to room temperature in water. The CDW state is characterized by a $2 \times 2 \times 2$ superstructure due to the dimerization of Ge1a atoms (see below). High-resolution single-crystal x-ray diffraction (SC-XRD) reveals a significant degree of disorder on the Ge1 sites in the high-T pristine phase of FeGe. This annealing-tunable disorder in the high-T phase holds the key to the fate of both the CDW and various magnetic orders. Experimental details can be found in the Supplemental Material [32].

As shown in Fig. 1(a), the in-plane magnetic susceptibility ($\chi_\perp$, $H \perp c$) of FeGe samples varies systematically as a function of annealing temperature, T_{Ann}. All discrepant behaviors reported in the literature so far can be reproduced by choosing an appropriate T_{Ann}. Notably, the annealing effect is highly repeatable and reversible. Similar results are obtained for crystals annealed at the same conditions, regardless of their annealing history [see Fig. 1(c)]. The overall behavior of the $T_{Ann} = 560$°C curve is similar to that reported decades ago by Bernhard *et al.* [28,29]: No clear signatures of a CDW transition can be identified. Only the AFM transition (a kink at $T_N = 398$ K), and multiple canting transitions (an upturn at $T_{canting} \sim 55$ K, a peak at $T'_{canting} \sim 37$ K, and a weak kink around $T''_{canting} \sim 6$ K), are found. Early neutron measurements suggest that below T_N, hexagonal FeGe adopts a c-axis A-type AFM structure, which transforms to a c-axis double cone AFM below $T_{canting}$ [29]. Changes in the cone angle produce a peak and a kink in $\chi_\perp$ at $T'_{canting}$ and $T''_{canting}$ [29].

For $T_{Ann} = 480$ °C, a CDW-induced broad jump appears in $\chi_\perp(T)$ around 100 K, similar to that reported by Teng *et al.* [10]. With further decreasing T_{Ann}, the CDW transition becomes much sharper, exhibiting an enhanced transition temperature (T_{CDW}) and amplitude of the jump in susceptibility ($\Delta\chi_\perp$). For $T_{Ann} < 320$ °C, the CDW transition becomes broad again since a longer annealing time would be required if T_{Ann} is lowered. The CDW transition is most pronounced for $T_{Ann} = 320$ °C, as reflected by the highest T_{CDW}, sharpest transition width, and the largest $\Delta\chi_\perp$. More importantly, instead of the short-range CDW reported before [10–12], a long-range CDW is realized in crystals annealed at 320 °C, as evidenced by the SC-XRD shown below in Fig. 3.

The magnetic orders are also sensitive to the annealing temperatures. The AFM transition temperature T_N shifts moderately by changing T_{Ann} [inset of Fig. 1(a)]. With a decrease in T_{Ann}, the canting transition at $T_{canting}$ becomes more evident, turning into a steplike feature for $T_{Ann} \leq 320$ °C. The transition at $T'_{canting}$ weakens and shifts below 2 K for $T_{Ann} \leq 320$ °C. Note that for $T_{Ann} \leq 320$ °C, an additional broad hump appears in $\chi_\perp(T)$ between 150 and 250 K, which can be eliminated by extending the annealing time [red curve in Fig. 1(c)]. Magnetization measurements (Figs. S7–S9 in Supplemental Material [32]) suggest that this broad hump is likely induced by a ferromagnetic transition at 250 K and a subsequent spin reorientation at 150 K. This behavior can be ascribed to a small amount ($< 0.1\%$) of annealing-induced magnetic clusters, which have their easy axis, within the ab plane between 250 and 150 K, rotating to the c axis below 150 K.

In Fig. 1(b), we summarize the annealing-tuned phase diagram. By varying T_{Ann}, T_N and T_{CDW} change systematically but with opposite trends: T_N/T_{CDW} reaches its minimum or maximum at $T_{Ann} = 320$ °C, indicating an anticorrelation between T_N and T_{CDW}, as seen more clearly in a T_N vs T_{CDW} plot [Fig. S1(f) in Supplemental Material [32]]. Crucially, as shown in Fig. 1(d), both T_N and T_{CDW} show a monotonic variation with the annealing-tuned c-axis lattice parameter, indicating a possible structural origin of their anticorrelation. From Fig. 1(b), it can be seen

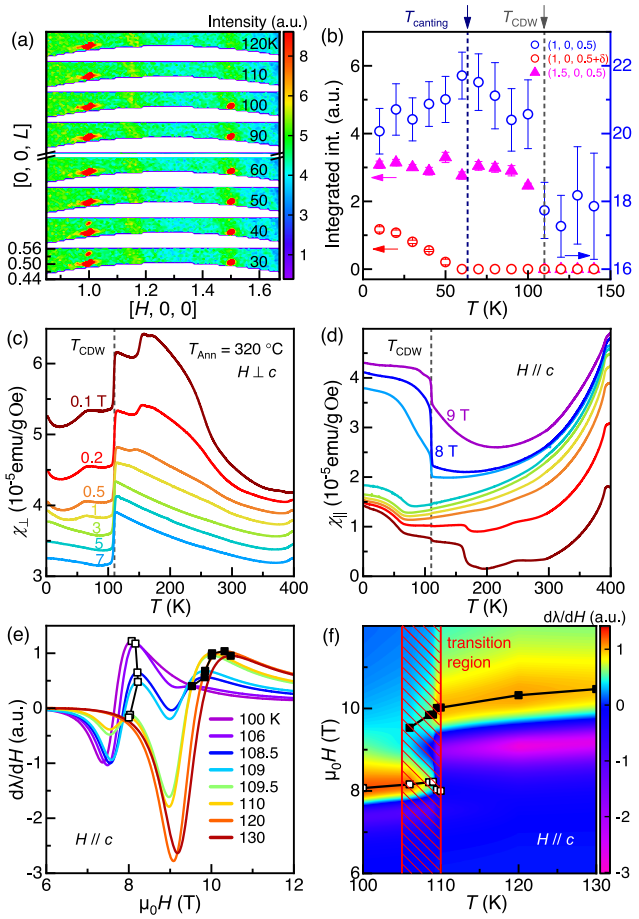

FIG. 2. (a) Neutron diffraction pattern of a FeGe crystal annealed at 320 °C, captured in the $[H, 0, L]$ plane. (b) Integrated intensities of the AFM peak (1, 0, 0.5), incommensurate magnetic peak (1, 0, $0.5 + \delta$), and CDW peak (1.5, 0, 0.5) derived from panel (a) data. Both y axes in panel (b) share the same scale. (c) and (d) Temperature-dependent in-plane and out-of-plane magnetic susceptibilities, respectively. (e) and (f) Magnetostriction coefficient $\mathrm{d}\lambda/\mathrm{d}H$ and the corresponding $H-T$ phase diagrams, with black squares indicating the spin-flop transition field H_{sf}.

that the evolution of T_{canting} and T'_{canting} as a function of T_{Ann} are similar to those of T_{CDW} and T_{N}, respectively. The origin of this similarity and the nature of spin-canting transitions will be explored in the following part of the Letter.

To elucidate the nature of the long-range CDW and its relationship with magnetic orders, we conducted single-crystal neutron diffraction, magnetization, and magnetostriction measurements on a 320 °C annealed crystal. As shown in Fig. 2(a), magnetic Bragg peaks associated with the A-type AFM structure are nicely resolved below T_{N} at the commensurate magnetic peak (1, 0, 0.5) within the (H, 0, L) plane [10,29,30]. Upon cooling below $T_{\mathrm{canting}} \sim 60$ K, additional incommensurate magnetic peaks appear at (1, 0, $0.5 \pm \delta$) with $\delta = 0.04$, signaling a transition to a double cone AFM configuration [10,29,30]. An intense peak at (1.5, 0, 0.5) appears just below $T_{\mathrm{CDW}} = 110$ K, indicating CDW formation [10]. The temperature-dependent peak intensities, shown in Fig. 2(b), reveal that the AFM peak intensity sharply increases below T_{CDW}, implying an intimate correlation between the CDW and magnetic orders [10]. Below T_{canting}, spin canting from the c axis towards the ab plane leads to gradual suppression (enhancement) in the intensity of the commensurate (incommensurate) magnetic peak, agreeing well with previous studies [10,29,30]. The modulation vector of the incommensurate magnetic peak is temperature independent and has almost the same value as that in samples with no CDW [29] or short-range CDW [10,60]. This result indicates that samples annealed at different temperatures share a similar low-temperature double-cone magnetic structure, with difference in the detailed spin canting transition attributed to variations of cone angles among samples (see Fig. S6 in Supplemental Material [32]). Note that the CDW peak intensity shows no anomaly around T_{canting}, indicating that the CDW is insensitive to the spin-canting transition.

The low-temperature magnetic structure changes significantly under external magnetic fields. Figures 2(c) and 2(d) show that the canting transition disappears above 1 T (5 T) for $H \perp c$ ($H \| c$). Additionally, the application of a magnetic field above 1 T eliminates the broad hump in susceptibility observed between 150 and 250 K in the low-field conditions, attributed to the saturation of the minor FM clusters. However, the CDW transition remains unaffected by high magnetic fields, even in the spin-flop phase above 7 T for $H \| c$. Below T_{CDW}, the susceptibility $\chi_{\|}$ increases sharply above 7 T, reflecting a reduction in the critical field (H_{sf}) for the spin-flop transition in the CDW state [see Fig. 2(d)]. The variation of H_{sf} upon the CDW transition is further elucidated through the magnetostriction measurements as depicted in Figs. 2(e) and 2(f). The relative magnetostrictive coefficient $\mathrm{d}\lambda/\mathrm{d}H$ (where $\lambda = \Delta L/L$, and L is the geometrical length of the sample), was measured by a novel composite magnetoelectric method [61]. Near the CDW transition, $\mathrm{d}\lambda/\mathrm{d}H$ exhibits two dip-peak features associated with the spin-flop transition [Fig. 2(e)]. On the other hand, only a single dip-peak feature is evident in $\mathrm{d}\lambda/\mathrm{d}H$ both below and above T_{CDW}. As summarized in Fig. 2(f), H_{sf} exhibits a sharp steplike jump, accompanied by a phase coexistence region near T_{CDW}, indicating the coexistence of high-temperature pristine and low-temperature CDW phases. This serves as compelling evidence for the first-order nature of the CDW transition. These findings suggest that the CDW is unaffected by changes in the magnetic structure, while H_{sf} is markedly reduced in the CDW phase.

Finally, our SC-XRD results are displayed in Fig. 3. Analysis of the 300 K crystallographic structure in space group $P6/mmm$ initially suggests a replication of known

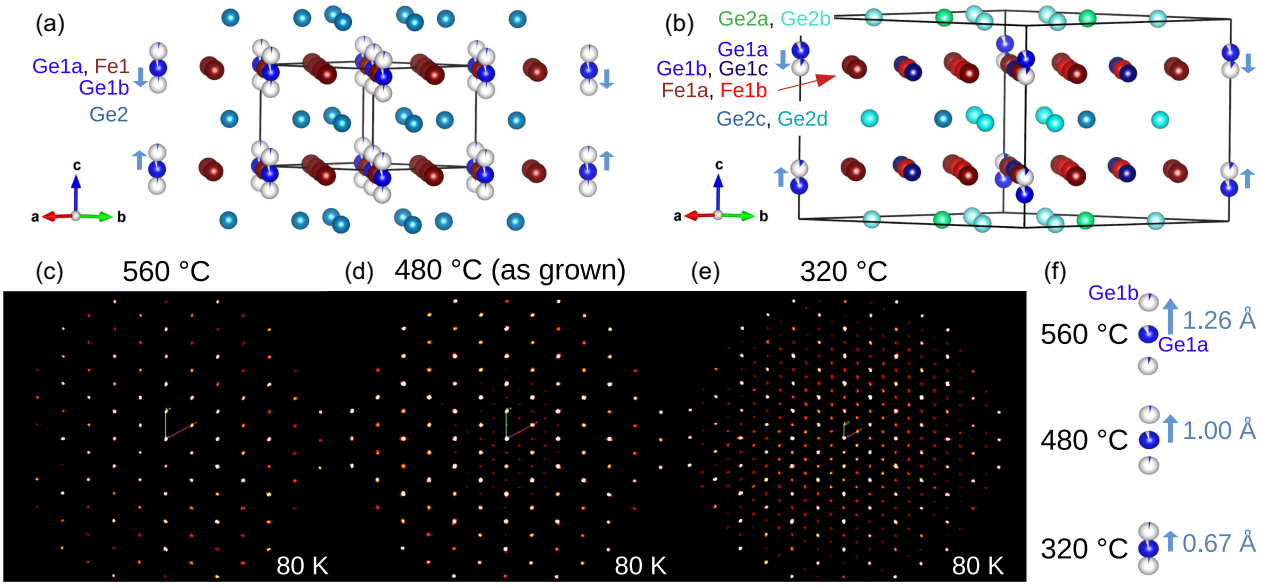

FIG. 3. (a) Crystal structure of pristine FeGe at 300 K. In addition to the established Ge1a (the Ge site in the Fe_3Ge plane), a disordered Ge1b site is found shifted along the crystallographic c axis as indicated by the light blue arrows. The degree of disorder strongly depends on the annealing conditions and is reflected in the occupancy of the disordered site and its distance to Ge1a as shown in (f). (b) $2 \times 2 \times 2$ CDW crystal structure of FeGe at 80 K realized only for samples annealed at 320 °C. To form the Ge1a-Ge1a dimers, the Ge1a atoms are moved upwards (downwards) from their initial positions. However, also for the low-T structure a disordered Ge1b site is found at the position where the Ge1a atoms initially reside at 300 K. (c),(d), and (e) Illustrate the RL view along the c^* direction measured at 80 K for samples annealed at 560, 480, and 320 °C, respectively. The high-T RL of all investigated samples looks essentially identical to the one in (c). (f) Distance at 300 K between Ge1b and Ge1a which is a reasonable indicator for the amount of disorder.

atomic positions. However, profound refinement of all samples indicates incomplete occupancy of the Ge1a site, i.e., of the Ge site within the Fe_3Ge plane. Difference Fourier analysis further reveals a significant residual electron density shift along the c axis away from the Ge1a site, as detailed in the Supplemental Material [32]. Inserting a Ge1b atom at this position, the discrepancy in Ge occupancy at the Ge1a site is precisely balanced by the Ge1b site (with and without restricting the sum of both sites to an occupation of 1), markedly improving refinement residuals, as outlined in the Supplemental Material [32]. Figure 3(a) illustrates the partially occupied Ge1a and the disordered Ge1b site. This finding unambiguously demonstrates that the high-T phase of FeGe features substantial disorder.

Most interestingly, the occupancy of the disordered Ge1b site and its distance to the Fe_3Ge plane strongly depend on the annealing conditions of the samples as illustrated in Fig. 3(f) and serve as a good indicator for the amount of disorder: Samples annealed at 560 °C, 480 °C, and 320 °C show occupancy of the disordered Ge1b site (of Ge1a) of 9% (91%), 6% (94%), and 5% (95%) and a distance to Ge1a of 1.259(9) Å, 1.00(2) Å, and 0.665(9) Å, respectively. Hence, with a higher annealing temperature, the disorder determined at 300 K strongly increases. Since SC-XRD averages over many unit cells, it is difficult to decide whether individual disordered Ge1b sites are statistically distributed over the sample or if they randomly occur in pairs in a unit cell. If in pairs, however, they could be interpreted as preformed Ge1b-Ge1b dimers locally existing already far above T_{CDW}, which would be consistent with what is observed for $FeGe_{1-x}Sb_x$ in Ref. [43].

The 80 K reciprocal lattice (RL) views along c^* plotted in Figs. 3(c)–3(e) exemplify that a long-range CDW and, thus, the low-T $2 \times 2 \times 2$ superstructure of FeGe shown in Fig. 3(b) is realized only for samples annealed at 320 °C. For samples annealed at 480 °C, only weak and more diffuse reflections characteristic for a short-range CDW are detected, whereas for samples annealed at 560 °C CDW reflections are completely absent. These observations indicate that the CDW volume fraction decreases with increasing T_{Ann}, consistent with the magnetization measurements (see Fig. 1). For samples annealed at 320 °C, the Ge1a atoms are moved upwards (downwards) from their initial positions at 300 K to form a 2×2 pattern of Ge1a-Ge1a dimers [Fig. 3(b)]. Remarkably, a disordered Ge1b position (occupation 0.08) shifted from the low-T Ge1a dimer position (occupation 0.92) is also found in this phase [Fig. 3(b)]. Together with the formation of Ge1a-Ge1a dimers, small but clear in-plane Kekulé-type distortions in the two Ge2 honeycomb layers and predominant out-of-plane buckling in the two Fe kagome layers can be observed (see Supplemental Material [32] for details). Apart from tiny in-plane movements of the Fe atoms

resolved in our data [32], these findings are consistent with theoretical predictions [21,26,62]. In contrast, the low-T structures of samples annealed at 480 and 560 °C are similar to their high-T phase with subtle variations in the Ge1b disorder [see Fig. 3(a)], resulting in an identical occupation of the Ge1b site (8.5% for both samples) and Ge1b-Ge1b distances between 2.46–2.69 Å. These low-T Ge1b-Ge1b bond lengths are close to the Ge1a-Ge1a dimer distance (2.72 Å) of 320 °C annealed samples and, therefore, perfectly fit into a dimer picture. Accordingly, a sound rationale for the variance in the CDW volume fraction lies in the distribution of the Ge1 dimers: Statistically for the 560 °C sample, clustered for the short-range CDW ordered 480 °C sample, and long-range 2×2 ordered for the genuine CDW phase of the 320 °C sample. A more detailed and complementing crystallographic discussion of all structural properties and atomic positions will be given in the Supplemental Material [32].

Our SC-XRD analysis thus reveals multiple energy minima for Ge1 atoms, characterized by specific distances (z) to the Fe_3Ge plane: Pristine Ge1a at $z = 0$, a range of positions for Ge1b with $z = 0.16$–0.3, and the Ge1a-Ge1a dimer at $z = 0.16$. These findings are consistent with predictions from double or triple-well potential models [26,27], which might be best captured in the framework of a multiwell potential model. The distribution of Ge1 atoms at 300 K is largely determined by the annealing conditions: Higher annealing temperatures increase the probability of Ge1 atoms populating metastable Ge1b sites, whereas lower annealing temperatures lead to the occupation of the slightly more stable pristine Ge1a sites. Consequently, high Ge1b disorder levels trap the system in local energy minima, hindering the transition to the possible lower-energy CDW state with 2×2 Ge1a-Ge1a dimers at low temperatures. Varying annealing conditions, however, can overcome the energy barrier between energy minima, allowing for repeatable and reversible ground state tuning, as evidenced in Fig. 1(c).

The annealing-tuned magnetic properties are also likely linked to the displacement of Ge1 atoms, significantly influencing the magnetic exchange interaction (J), anisotropy (K), and spin splitting or polarization. The displacement of Ge1b atoms away from the Fe_3Ge plane leads to a more three-dimensional (3D) structure, potentially enhancing the interlayer J_c and reducing K. This is evidenced by the increase of T_N with higher annealing temperatures [Fig. 1(b)], mirroring trends observed in van der Waals layered magnets [49,63]. Consequently, the observed anti-correlation between T_N and T_{CDW} may stem from their distinct relationships with Ge1b disorder. The increased magnetic moment (decreased H_{sf}) in the CDW phase is most probably due to Ge1-distortion-induced enhancement of spin splitting or polarization (suppression of magnetic anisotropy) [21,26]. Furthermore, Ge1 disorder, which locally breaks the inversion symmetry, could induce finite Dzyaloshinskii-Moriya interaction. This offers a natural explanation for the observed symmetry-forbidden double cone magnetic structure at low temperatures and the persistence of incommensurate spin excitations up to at least 350 K [60,62]. The spin canting transition is thus tied with the Ge1 displacements. In samples dominated by the CDW phase ($T_{Ann} \leq 360$ °C), $T_{canting}$ exhibits a similar T_{Ann} dependency as T_{CDW}, while it resembles the one of T_N in samples dominated by Ge1b disorder ($T_{Ann} \geq 400$°C). These findings suggest that structural factors play a dominant role in FeGe, with magnetism possibly being a secondary effect. This is similar to the structurally dominated CDW observed in non-magnetic materials such as ScV_6Sn_6 and $IrTe_2$ [64–66].

In conclusion, our study demonstrates that annealing treatments can reversibly tune both the CDW and magnetic orders in FeGe. The annealing-induced variation of CDW and magnetic orders, as well as their relationship, are closely linked to Ge1 atom displacement, which is adjustable through annealing. This study offers a notable method for achieving a long-range CDW in FeGe, emphasizes the predominant influence of structural factors, and sets important constraints on the theoretical understanding of the CDW mechanism.

We thank Ya-Jun Yan, Yilin Wang, Yuan Li, Christoph Meingast, Matthieu Le Tacon, and Weijun Ren for their helpful discussions. This work was supported by the Natural Science Foundation of China (No. 12374081, No. 12227806, and No. 12004056.) A. W. acknowledges the support from Chongqing Research Program of Basic Research and Frontier Technology, China (Grant No. cstc2021jcyj-msxmX0661). Y. S. C. acknowledges the support from the Beijing National Laboratory for Condensed Matter Physics. M. He acknowledges the support by Chinesisch-Deutsche Mobilitätsprogamm of Chinesisch-Deutsche Zentrum für Wissenschaftsförderung (Grant No. M-0496). We would like to thank Guiwen Wang and Yan Liu at the Analytical and Testing Center of Chongqing University and Siegmar Roth and Andre Beck at the Institute for Quantum Materials and Technologies, Karlsruhe Institute of Technology for their technical assistance. We are grateful to the beamtime on WOMBAT at the OPAL facility.

*These authors contributed equally to this work.
†mingquan.he@cqu.edu.cn
‡michael.merz@kit.edu
§yschai@cqu.edu.cn
‖afwang@cqu.edu.cn

[1] K. Jiang, T. Wu, J.-X. Yin, Z. Wang, M. Z. Hasan, S. D. Wilson, X. Chen, and J. Hu, Kagome superconductors AV_3Sb_5 (A = K, Rb, Cs), Natl. Sci. Rev. **10**, nwac199 (2022).
[2] J.-X. Yin, B. Lian, and M. Z. Hasan, Topological kagome magnets and superconductors, Nature (London) **612**, 647 (2022).

[3] T. Neupert, M. M. Denner, J.-X. Yin, R. Thomale, and M. Z. Hasan, Charge order and superconductivity in kagome materials, Nat. Phys. **18**, 137 (2022).

[4] B. R. Ortiz, L. C. Gomes, J. R. Morey, M. Winiarski, M. Bordelon, J. S. Mangum, I. W. H. Oswald, J. A. Rodriguez-Rivera, J. R. Neilson, S. D. Wilson, E. Ertekin, T. M. McQueen, and E. S. Toberer, New kagome prototype materials: Discovery of KV_3Sb_5, RbV_3Sb_5, and CsV_3Sb_5, Phys. Rev. Mater. **3**, 094407 (2019).

[5] B. R. Ortiz, S. M. L. Teicher, Y. Hu, J. L. Zuo, P. M. Sarte, E. C. Schueller, A. M. Milinda Abeykoon, M. J. Krogstad, S. Rosenkranz, R. Osborn, R. Seshadri, L. Balents, J. He, and S. D. Wilson, CsV_3Sb_5: A $\mathbb{Z}_2$ topological kagome metal with a superconducting ground state, Phys. Rev. Lett. **125**, 247002 (2020).

[6] B. R. Ortiz, P. M. Sarte, E. M. Kenney, M. J. Graf, S. M. L. Teicher, R. Seshadri, and S. D. Wilson, Superconductivity in the $\mathbb{Z}_2$ kagome metal KV_3Sb_5, Phys. Rev. Mater. **5**, 034801 (2021).

[7] Q. Yin, Z. Tu, C. Gong, Y. Fu, S. Yan, and H. Lei, Superconductivity and normal-state properties of kagome metal RbV_3Sb_5 single crystals, Chin. Phys. Lett. **38**, 037403 (2021).

[8] L. Nie *et al.*, Charge-density-wave-driven electronic nematicity in a kagome superconductor, Nature **604**, 59 (2022).

[9] H. Chen *et al.*, Roton pair density wave in a strong-coupling kagome superconductor, Nature (London) **599**, 222 (2021).

[10] X. Teng *et al.*, Discovery of charge density wave in a kagome lattice antiferromagnet, Nature (London) **609**, 490 (2022).

[11] J.-X. Yin *et al.*, Discovery of charge order and corresponding edge state in kagome magnet FeGe, Phys. Rev. Lett. **129**, 166401 (2022).

[12] Z. Chen, X. Wu, R. Yin, J. Zhang, S. Wang, Y. Li, M. Li, A. Wang, Y. Wang, Y.-J. Yan, and D.-L. Feng, Charge density wave with strong quantum phase fluctuations in kagome magnet FeGe, arXiv:2302.04490.

[13] H. Tan, Y. Liu, Z. Wang, and B. Yan, Charge density waves and electronic properties of superconducting kagome metals, Phys. Rev. Lett. **127**, 046401 (2021).

[14] G. Liu, X. Ma, K. He, Q. Li, H. Tan, Y. Liu, J. Xu, W. Tang, K. Watanabe, T. Taniguchi, L. Gao, Y. Dai, H.-H. Wen, B. Yan, and X. Xi, Observation of anomalous amplitude modes in the kagome metal CsV_3Sb_5, Nat. Commun. **13**, 3461 (2022).

[15] Y. Xie, Y. Li, P. Bourges, A. Ivanov, Z. Ye, J.-X. Yin, M. Z. Hasan, A. Luo, Y. Yao, Z. Wang, G. Xu, and P. Dai, Electron-phonon coupling in the charge density wave state of CsV_3Sb_5, Phys. Rev. B **105**, L140501 (2022).

[16] Y. Zhong, S. Li, H. Liu, Y. Dong, Y. Arai, H. Li, Y. Shi, Z. Wang, S. Shin, H. N. Lee *et al.*, Testing electron-phonon coupling for the superconductivity in kagome metal CsV_3Sb_5, Nat. Commun. **14**, 1945 (2023).

[17] M. Kang, S. Fang, J.-K. Kim, B. R. Ortiz, S. H. Ryu, J. Kim, J. Yoo, G. Sangiovanni, D. D. Sante, B.-G. Park, C. Jozwiak, A. Bostwick, E. Rotenberg, E. Kaxiras, S. D. Wilson, J.-H. Park, and R. Comin, Twofold van hove singularity and origin of charge order in topological kagome superconductor CsV_3Sb_5, Nat. Phys. **18**, 301 (2022).

[18] X. Zhou, Y. Li, X. Fan, J. Hao, Y. Dai, Z. Wang, Y. Yao, and H.-H. Wen, Origin of charge density wave in the kagome metal CsV_3Sb_5 as revealed by optical spectroscopy, Phys. Rev. B **104**, L041101 (2021).

[19] Z. Chen, X. Wu, S. Zhou, J. Zhang, R. Yin, Y. Li, M. Li, J. Gong, M. He, Y. Chai, X. Zhou, Y. Wang, A. Wang, Y.-J. Yan, and D.-L. Feng, Long-ranged charge order conspired by magnetism and lattice in an antiferromagnetic kagome metal, arXiv:2307.07990.

[20] H. Miao, T. T. Zhang, H. X. Li, G. Fabbris, A. H. Said, R. Tartaglia, T. Yilmaz, E. Vescovo, J.-X. Yin, S. Murakami, X. L. Feng, K. Jiang, X. L. Wu, A. F. Wang, S. Okamoto, Y. L. Wang, and H. N. Lee, Signature of spin-phonon coupling driven charge density wave in a kagome magnet, Nat. Commun. **14**, 6183 (2023).

[21] S. Shao, J.-X. Yin, I. Belopolski, J.-Y. You, T. Hou, H. Chen, Y. Jiang, M. S. Hossain, M. Yahyavi, C.-H. Hsu, Y. P. Feng, A. Bansil, M. Z. Hasan, and G. Chang, Intertwining of magnetism and charge ordering in kagome FeGe, ACS Nano **17**, 10164 (2023).

[22] X. Teng, J. S. Oh, H. Tan, L. Chen, J. Huang, B. Gao, J.-X. Yin, J.-H. Chu, M. Hashimoto, D. Lu, C. Jozwiak, A. Bostwick, E. Rotenberg, G. E. Granroth, B. Yan, R. J. Birgeneau, P. Dai, and M. Yi, Magnetism and charge density wave order in kagome FeGe, Nat. Phys. **19**, 814 (2023).

[23] L. Wu, Y. Hu, D. Fan, D. Wang, and X. Wan, Electron-correlation-induced charge density wave in FeGe, Chin. Phys. Lett. **40**, 117103 (2023).

[24] H.-Y. Ma, J.-X. Yin, M. Zahid Hasan, and J. Liu, Theory for charge density wave and orbital-flux state in antiferromagnetic kagome metal FeGe, Chin. Phys. Lett. **41**, 047103 (2024).

[25] Z. Zhao, T. Li, P. Li, X. Wu, J. Yao, Z. Chen, S. Cui, Z. Sun, Y. Yang, Z. Jiang, Z. Liu, A. Louat, T. Kim, C. Cacho, A. Wang, Y. Wang, D. Shen, J. Jiang, and D. Feng, Photoemission evidence of a novel charge order in kagome metal FeGe, arXiv:2308.08336.

[26] Y. Wang, Enhanced spin-polarization via partial Ge-dimerization as the driving force of the charge density wave in FeGe, Phys. Rev. Mater. **7**, 104006 (2023).

[27] B. Zhang, J. Ji, C. Xu, and H. Xiang, Triple-well charge density wave transition driven by cooperation between peierls-like effect and antiferromagnetic order in FeGe, arXiv:2307.10565.

[28] O. Beckman, K. Carrander, L. Lundgren, and M. Richardson, Susceptibility measurements and magnetic ordering of hexagonal FeGe, Phys. Scr. **6**, 151 (1972).

[29] J. Bernhard, B. Lebech, and O. Beckman, Neutron diffraction studies of the low-temperature magnetic structure of hexagonal FeGe, J. Phys. F **14**, 2379 (1984).

[30] J. Bernhard, B. Lebech, and O. Beckman, Magnetic phase diagram of hexagonal FeGe determined by neutron diffraction, J. Phys. F **18**, 539 (1988).

[31] H. Watanabe and N. Kunitomi, On the neutron diffraction study of FeGe, J. Phys. Soc. Jpn. **21**, 1932 (1966).

[32] See Supplemental Material at http://link.aps.org/supplemental/10.1103/PhysRevLett.132.256501, which includes Refs. [33–59], for the experimental details including

single-crystal growth, annealing treatments, structural characterization, neutron, magnetization, and magnetostrictive coefficient measurements.

[33] K. Ishii, S. Asano, M. Ashida, M. Fujita, B. Yu, M. Greven, J. Okamoto, D.-J. Huang, and J. Mizuki, Post-growth annealing effects on charge and spin excitations in $Nd_{2-x}Ce_xCuO_4$, Phys. Rev. Mater. **5**, 024803 (2021).

[34] C. R. Rotundu, B. Freelon, T. R. Forrest, S. D. Wilson, P. N. Valdivia, G. Pinuellas, A. Kim, J.-W. Kim, Z. Islam, E. Bourret-Courchesne, N. E. Phillips, and R. J. Birgeneau, Heat capacity study of $BaFe_2As_2$: Effects of annealing, Phys. Rev. B **82**, 144525 (2010).

[35] S. Ran, S. L. Bud'ko, D. K. Pratt, A. Kreyssig, M. G. Kim, M. J. Kramer, D. H. Ryan, W. N. Rowan-Weetaluktuk, Y. Furukawa, B. Roy, A. I. Goldman, and P. C. Canfield, Stabilization of an ambient-pressure collapsed tetragonal phase in $CaFe_2As_2$ and tuning of the orthorhombic-antiferromagnetic transition temperature by over 70 K via control of nanoscale precipitates, Phys. Rev. B **83**, 144517 (2011).

[36] Y. Sun, Z. Shi, and T. Tamegai, Review of annealing effects and superconductivity in $Fe_{1+y}Te_{1-x}Se_x$ superconductors, Supercond. Sci. Technol. **32**, 103001 (2019).

[37] C. J. Sayers, L. S. Farrar, S. J. Bending, M. Cattelan, A. J. H. Jones, N. A. Fox, G. Kociok-Köhn, K. Koshmak, J. Laverock, L. Pasquali, and E. Da Como, Correlation between crystal purity and the charge density wave in 1T-VSe_2, Phys. Rev. Mater. **4**, 025002 (2020).

[38] S. Ishida, T. Liang, M. Nakajima, K. Kihou, C. H. Lee, A. Iyo, H. Eisaki, T. Kakeshita, T. Kida, M. Hagiwara, Y. Tomioka, T. Ito, and S. Uchida, Manifestations of multiple-carrier charge transport in the magnetostructurally ordered phase of $BaFe_2As_2$, Phys. Rev. B **84**, 184514 (2011).

[39] C. P. Adams, T. E. Mason, S. A. M. Mentink, and E. Fawcett, The magnetic phase diagram and transport properties of $FeGe_2$, J. Phys. Condens. Matter **9**, 1347 (1997).

[40] G. M. Sheldrick, A short history of SHELX, Acta Crystallogr. Sect. A **64**, 112 (2008).

[41] G. M. Sheldrick, Crystal structure refinement with SHELXL, Acta Crystallogr. C **71**, 3 (2015).

[42] V. Petříček, M. Dušek, and L. Palatinus, Crystallographic computing system JANA2006: General features, Z. Kristallogr. Cryst. Mater. **229**, 345 (2014).

[43] J. Huang, C. Shang, J. Qin, F. Pan, B. Shi, J. Wang, J. Liu, D. Xu, H. Zhang, H. Wang, L. Hao, W. Bao, and P. Cheng, $FeGe_{1-x}Sb_x$: A series of kagome metals with noncollinear antiferromagnetism, Phys. Rev. B **108**, 184431 (2023).

[44] Hasitha W. Suriya Arachchige, W. R. Meier, M. Marshall, T. Matsuoka, R. Xue, M. A. McGuire, R. P. Hermann, H. Cao, and D. Mandrus, Charge density wave in kagome lattice intermetallic ScV_6Sn_6, Phys. Rev. Lett. **129**, 216402 (2022).

[45] C. Shi *et al.*, Disordered structure for long-range charge density wave order in annealed crystals of magnetic kagome FeGe, arXiv:2308.09034.

[46] J. B. Forsyth, C. Wilkinson, and P. Gardner, The low-temperature magnetic structure of hexagonal FeGe, J. Phys. F **8**, 2195 (1978).

[47] H. Li, Y. Liu, L. Xie, Y. Guo, Z. Ma, Y. Li, X. He, L. Liu, and H. Zhang, The spin-reorientation magnetic transitions in Ga-doped $SmCrO_3$, Ceram. Int. **44**, 18913 (2018).

[48] P. Mandal, V. S. Bhadram, Y. Sundarayya, C. Narayana, A. Sundaresan, and C. N. R. Rao, Spin-reorientation, ferroelectricity, and magnetodielectric effect in $YFe_{1-x}Mn_xO_3$ ($0.1 \leq x \leq 0.40$), Phys. Rev. Lett. **107**, 137202 (2011).

[49] J. Seo *et al.*, Nearly room temperature ferromagnetism in a magnetic metal-rich van der Waals metal, Sci. Adv. **6**, eaay8912 (2020).

[50] L. Xu, H. Han, J. Fan, D. Shi, D. Hu, H. Du, L. Zhang, Y. Zhang, and H. Yang, Magnetic entropy change and accurate determination of Curie temperature in single-crystalline helimagnet FeGe, Europhys. Lett. **117**, 47004 (2017).

[51] L. Ludgren, O. Beckman, V. Attia, S. P. Bhattacheriee, and M. Richardson, Helical spin arrangement in cubic FeGe, Phys. Scr. **1**, 69 (1970).

[52] G. P. Felcher and J. D. Jorgensen, Magnetic structures of monoclinic FeGe, J. Phys. C **16**, 6281 (1983).

[53] D. Oleszak, E. Jartych, A. Antolak, M. Pekala, M. Szymanska, and M. Budzynski, Structure, hyperfine interactions and magnetization studies of mechanically alloyed $Fe_{50}Ge_{50}$ and $Fe_{62}Ge_{38}$, J. Alloys Compd. **400**, 23 (2005).

[54] K. Kanematsu and T. Ohoyama, Magnetic and x-ray studies of iron-germanium system II. Phase diagram and magnetism of each phase, J. Phys. Soc. Jpn. **20**, 236 (1965).

[55] W.-Y. Wu, W. W. Tjiu, W. Wan, H. R. Tan, S. L. Teo, S. Guo, S. T. Lim, and M. Lin, Endotaxial growth of Fe_xGe single-crystals on Ge(001) substrates, CrystEngComm **20**, 2916 (2018).

[56] R. A. Khalaniya, V. Y. Verchenko, A. V. Sobolev, I. A. Presniakov, Z. Wei, E. V. Dikarev, and A. V. Shevelkov, Intricate magnetic behavior of Fe_6Ge_5 and its origin within a complex iron framework: The magnetic and ^{57}Fe Mössbauer study, J. Alloys Compd. **902**, 163759 (2022).

[57] V. Y. Verchenko, Z. Wei, A. A. Tsirlin, C. Callaert, A. Jesche, J. Hadermann, E. V. Dikarev, and A. V. Shevelkov, Crystal growth of the nowotny chimney ladder phase Fe_2Ge_3: Exploring new Fe-based narrow-gap semiconductor with promising thermoelectric performance, Chem. Mater. **29**, 9954 (2017).

[58] G. E. Grechnev, A. A. Lyogenkaya, V. A. Desnenko, A. V. Fedorchenko, and A. S. Panfilov, Magnetic and magnetoelastic properties of antiferromagnet $FeGe_2$, Low Temp. Phys. **49**, 1025 (2023).

[59] F. Albertini, D. Negri, L. Pareti, E. B. Watts, Z. Arnold, J. Kamarad, G. Calestani, A. Deriu, and S. Besseghini, Magnetocrystalline anisotropy of Fe_3Ge single crystal: Effect of pressure and Mn substitution for Fe, J. Appl. Phys. **96**, 2110 (2004).

[60] L. Chen, X. Teng, H. Tan, B. L. Winn, G. E. Granroth, F. Ye, D. H. Yu, R. A. Mole, B. Gao, B. Yan, M. Yi, and P. Dai, Competing itinerant and local spin interactions in kagome metal FeGe, Nat. Commun. **15**, 1918 (2024).

[61] Y. Chai, P. Lu, H. Du, J. Shen, Y. Ma, K. Zhai, L. Wang, Y. Shi, H. Li, W. Wang, and Y. Sun, Probe of skyrmion phases and dynamics in MnSi via the magnetoelectric effect in a composite configuration, Phys. Rev. B **104**, L100413 (2021).

[62] H. Zhou, S. Yan, D. Fan, D. Wang, and X. Wan, Magnetic interactions and possible structural distortion in kagome

FeGe from first-principles calculations and symmetry analysis, Phys. Rev. B **108**, 035138 (2023).

[63] J.-Q. Yan, Y. H. Liu, D. S. Parker, Y. Wu, A. A. Aczel, M. Matsuda, M. A. McGuire, and B. C. Sales, A-type antiferromagnetic order in $MnBi_4Te_7$ and $MnBi_6Te_{10}$ single crystals, Phys. Rev. Mater. **4**, 054202 (2020).

[64] S. Lee, C. Won, J. Kim, J. Yoo, S. Park, J. Denlinger, C. Jozwiak, A. Bostwick, E. Rotenberg, R. Comin, M. Kang, and J.-H. Park, Nature of charge density wave in kagome metal ScV_6Sn_6, npj Quantum Mater. **9**, 15 (2024).

[65] H. Tan and B. Yan, Abundant lattice instability in kagome metal ScV_6Sn_6, Phys. Rev. Lett. **130**, 266402 (2023).

[66] K. Kim, S. Kim, K.-T. Ko, H. Lee, J.-H. Park, J. J. Yang, S.-W. Cheong, and B. Min, Origin of first-order-type electronic and structural transitions in $IrTe_2$, Phys. Rev. Lett. **114**, 136401 (2015).